UDC 551.465.755:551.466.4:532.5

THE USE OF OPEN BOUNDARY CONDITIONS WITH THE STORM-SURGE EQUATIONS

M. G. WURTELE and JAN PAEGLE [1]
University of California, Los Angeles, Calif.

ANITA SIELECKI
Hebrew University, Jerusalem, Israel

ABSTRACT

Open boundaries are desirable when the region of interest of a computation is a localized area of a much larger domain. Boundary conditions are developed for the linear storm-surge equations (without Coriolis effects) that permit disturbances to pass out of the region of computation with negligible reflection. These conditions, based on the concept of Riemann invariants, are applied in one- and two-space dimensions. Examples of the flow around a sea mound, a shelf, and an island are given. Selected comparisons are made with Sommerfeld's radiation condition, advanced by Vastano and Reid.

1. INTRODUCTION

A very common problem in hydrodynamical computations arises when the theoretical model applies to an infinite or semi-infinite region. It then becomes necessary in the computation to represent one or more boundaries where none exists in the model (or in nature). This false boundary must have some sort of conditions applied along it, and it is generally the case that these conditions contaminate the computation and produce unreal results within the region. A common solution to the problem is to make the region so large that the boundary errors are propagated only through a small portion of it. However, aside from being wasteful and inelegant, this technique is inapplicable when the computation is two- or three-dimensional and the program approaches the capacity of the computer storage. The following is an account of the testing of some techniques, including two based on dynamical principles rather than computational ad hoc devices.

The equations integrated are those governing hydrostatic surface waves, often referred to as the "storm-surge equations":

$$\frac{\partial \eta}{\partial t}=-\left(\frac{\partial U}{\partial x}+\frac{\partial V}{\partial y}\right), \tag{1}$$

$$\frac{\partial U}{\partial t}=-gh(x,y)\frac{\partial \eta}{\partial x}+F_x, \tag{2}$$

and

$$\frac{\partial V}{\partial t}=-gh(x,y)\frac{\partial \eta}{\partial y}+F_y. \tag{3}$$

Here, η is interpreted as the wave height; U, the mass transport in the x direction; V, the mass transport in the y direction; h, the mean depth of the water; g, the acceleration due to gravity; and F_x, F_y, the forces applied to the water surface by the atmosphere.

For the finite-difference analog, the time and space differencing used to represent eq (1), (2), and (3) is

$$\Delta_n \eta^n_{j,k}=-\frac{\Delta t}{2\Delta s}\left(\delta_j U^n_{j,k}+\delta_k V^n_{j,k}\right), \tag{4}$$

$$\Delta_n U^n_{j,k}=-gh_{j,k}\frac{\Delta t}{2\Delta s}\,\delta_j \eta^{n+1}_{j,k}, \tag{5}$$

and

$$\Delta_n V^n_{j,k}=-gh_{j,k}\frac{\Delta t}{2\Delta s}\,\delta_k \eta^{n+1}_{j,k} \tag{6}$$

where Δ is the forward difference operator; δ, the centered difference operator; the indices (j, k, n) denote a point $(x, y, t)=(j\Delta x, k\Delta y, n\Delta t)$ of the discrete grid; and $\Delta x=\Delta y=\Delta s$. This difference scheme has been extensively tested by Sielecki (1968).

This scheme cannot be used at the boundaries because centered space differences normal to the boundary cannot be computed there. Before advancing the methods to be used for boundary conditions, it is helpful to examine the form of the analytic solution of the wave equation in two-space dimensions.

In the case of constant depth and zero force F, an analytic solution in terms of initial conditions may be obtained (Garabedian 1964, pp. 191–210):

$$\eta(x,y,t)=\frac{1}{c}\frac{\partial}{\partial t}\frac{1}{2\pi}\iint\frac{G_1(x+\zeta_1,\,y+\zeta_2)}{\sqrt{c^2t^2-\zeta_1^2-\zeta_2^2}}\,d\zeta_1 d\zeta_2 + \frac{1}{2\pi c}\iint\frac{G_2(x+\zeta_1,\,y+\zeta_2)}{\sqrt{c^2t^2-\zeta_1^2-\zeta_2^2}}\,d\zeta_1 d\zeta_2 \tag{7a}$$

where $\zeta_1^2+\zeta_2^2<c^2t^2$, $c=(gh)^{1/2}$, $G_1=\eta(x,y,0)$, and $G_2=\eta_t(x,y,0)$. This represents the solution at any point and time as an area integral over the circular domain of dependence cut from the initial data plane by the characteristic cone

$$(x-x_0)^2+(y-y_0)^2-c^2(t-t_0)^2=0.$$

[1] Present affiliation: Department of Meteorology, University of Utah, Salt Lake City

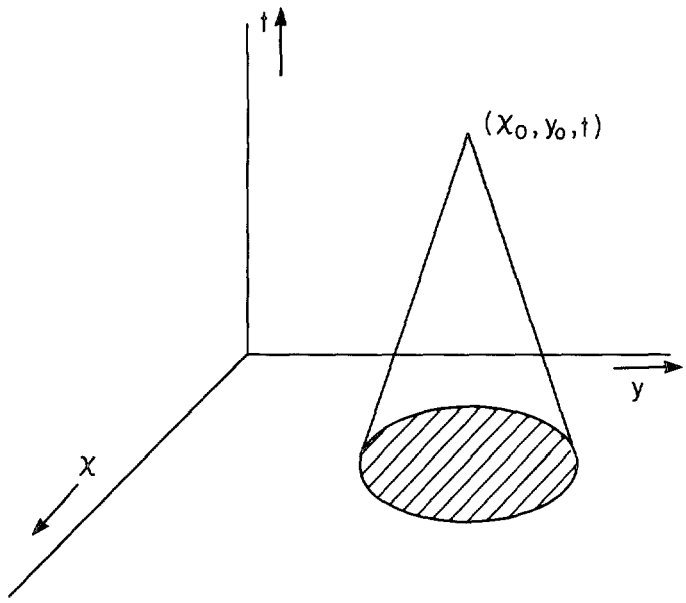

FIGURE 1.—Domain of dependence of the wave equation in two-space dimensions.

This is illustrated in figure 1. In one-space dimension eq (7a) simplifies to the familiar d'Alembert solution

$$\eta=\tfrac{1}{2}[G_1(x+ct)+G_1(x-ct)]+\tfrac{1}{2}\int_{-ct}^{ct} G_2(x+\xi)d\xi. \quad (7b)$$

We note first that, in two-space dimensions, after the disturbance has reached an arbitrary point in space, it never completely dies out there, regardless of how sharp or concentrated the initial disturbance may have been. Thus, if the point in question is an open boundary point, the disturbance outside that point will affect the interior region at all times; and the interior solution will be highly sensitive to the artificial boundary condition applied. In one-space dimension d'Alembert's solution shows that the same will be true in the general case. If, however, the initial tendency G_2 is zero, a concentrated initial disturbance propagates without change in shape; and an arbitrary point returns to its undisturbed condition once this disturbance passes it by.

These remarks illustrate the failure of Huygen's principle in two- (or any even number of) space dimensions, and its limited applicability in one-space dimension (see Garabedian 1964, p. 197).

Direct numerical quadrature of eq (7) would, of course, be possible. However, more general numerical procedures are desirable that permit variable mean depth h and arbitrary force distributions F.

2. AD HOC NUMERICAL TECHNIQUES

It might be thought at first that the most simple and straightforward scheme for the boundaries would be to take some sort of one-sided space derivatives at boundary points. However, a backward space difference in eq (2) or (3) is unstable, and this remains true even when this difference is taken only at a single boundary point. We may easily see this in the one-dimensional case. Let η^n and U^n be the boundary values at, say, $j=J$. These values would be computed by the one-sided differences

$$\eta^{n+1}-\eta^n=-\epsilon\left(\frac{\Delta t}{2\Delta x}\right)(U^n-U^n_{J-1}) \quad (8a)$$

and

$$U^{n+1}-U^n=-gh\epsilon\left(\frac{\Delta t}{2\Delta x}\right)(\eta^{n+1}-\eta^{n+1}_{J-1}) \quad (8b)$$

where ϵ is at our disposal. The differencing for the boundary point η^n, U^n is unstable if $\epsilon>0$, and the coupling with the interior points will subject that region to these instabilities. If $\epsilon<0$, the differencing is stable, but the effect is equivalent to the substitution $\partial/\partial x=-\partial/\partial x$, so that disturbances will be propagated back into the interior. This situation is analogous to that described by Platzman (1954) in his analysis of instabilities arising out of the first-order equation for vorticity advection with open boundaries.

The above conclusions were tested and confirmed by several experiments, in all of which the level of the water rose without limit.

3. DYNAMICALLY BASED METHODS

We now turn to the formulation of an exact condition for open boundaries in one-space dimension. The equations

$$\frac{\partial U}{\partial t}=-c^2\frac{\partial \eta}{\partial x}, \qquad \frac{\partial \eta}{\partial t}=-\frac{\partial U}{\partial x}, \qquad c^2=gh=\text{const}$$

may, upon multiplying the latter by c, be added and subtracted to obtain

$$\frac{\partial}{\partial t}(U+c\eta)+c\frac{\partial}{\partial x}(U+c\eta)=0 \quad (9a)$$

and

$$\frac{\partial}{\partial t}(U-c\eta)-c\frac{\partial}{\partial x}(U-c\eta)=0. \quad (9b)$$

The quantities $U\pm c\eta$ may be called the linearized Riemann invariants (cf. Garabedian 1964, pp. 509 ff., where the nonlinear case is discussed). Equations (9) state that these invariants are respectively conserved along the directions $dx/dt=\pm c$, that is, along the straight lines, called characteristics, $x\pm ct=$const in the (x,t) plane. In figure 2, characteristics have been drawn intersecting open boundaries assumed at $x=0$, L. It is clear that, at $x=0$, the appropriate boundary condition is the specification of $U+c\eta$ at all times; similarly, at $x=L$, $U-c\eta$ must be specified at all times. These are dynamic constraints representing the influence from outside the region $(0,L)$. If, say, η is computed at each boundary by a one-sided difference, U may be determined by the application of

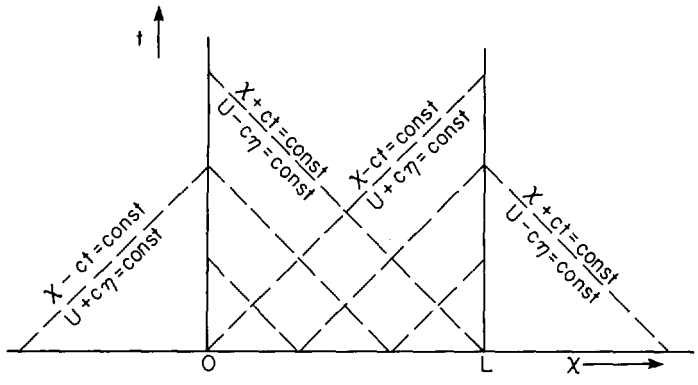

FIGURE 2.—Characteristics of the wave equation in one-space dimension.

these constraints. The following experiment will make this process clear.

EXPERIMENT 1

For the initial condition consisting of a lump of water between (0, L) with no initial disturbance outside, the conditions are obviously

$$U+c\eta=0 \quad x=0$$

and

$$U-c\eta=0 \quad x=L.$$

Since these conditions are exact, we should expect in the solution only the usual errors arising out of truncation. That this is the case is verified in figure 3. The computed and theoretical disturbance agree within a root mean square (rms) error of 1 percent.

When the model is extended to two-space dimensions, it becomes necessary to introduce approximations, there being no analog of the Riemann invariants. If, however, our finite-difference grid has a scale that is small compared to the radius of curvature of the wave fronts, we may treat the wave front reaching a given boundary point as locally a plane wave arriving from a direction specified by the transport components at that point. Stated otherwise, we specify for all times one of the quantities $\sqrt{U^2+V^2}\pm c\eta$ at the boundaries, the sign ambiguity being resolved accordingly as the point is an inflow (+) or outflow (−) point. Since this is an approximation introducing other errors than the well-understood truncation errors, we have tested the scheme under a variety of conditions. This method has been used by Trulio and Walitt (1970) for nonlinear compressible flow. However, they maintain $\eta=0$ at open boundaries, which is an inadequate condition for the linear case.

EXPERIMENT 2

The two-dimensional lump of water with zero initial disturbance outside requires the condition

$$\sqrt{U^2+V^2}-c\eta=0 \qquad (10)$$

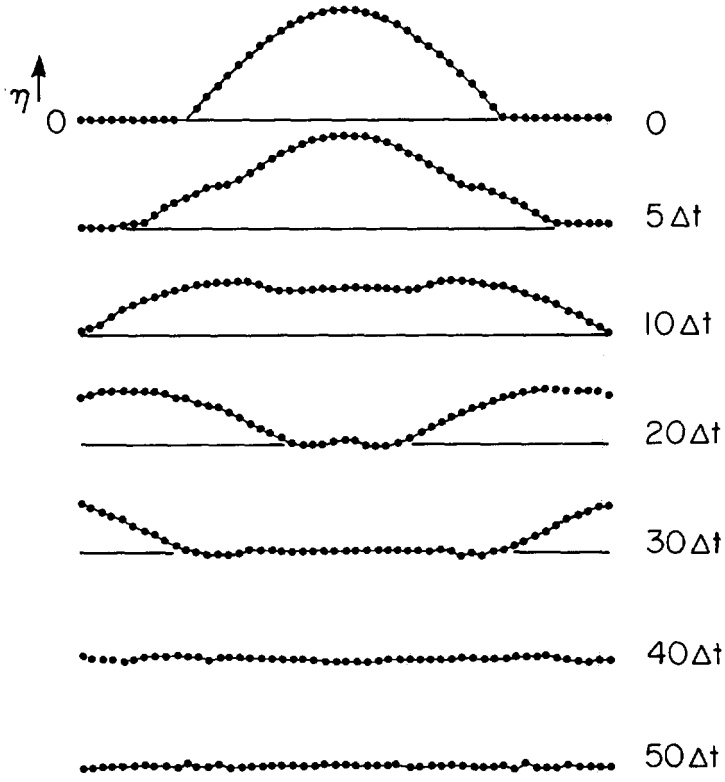

FIGURE 3.—Experiment 1, time evolution in one dimension of the free surface from the initial conditions $\eta=\cos(\pi j/30)$ for $|j-25|\leq 15$ and $\eta=0$ otherwise.

on all boundaries. This was used to determine the displacement η, the transports being computed from backward space differences. To maintain radial symmetry and allow specification of a flat initial field outside, the initial values of η were set equal to zero outside a radius of 13 grid points. The results appear quite reasonable and show no instability and very weak reflection (fig. 4).

An analytic solution for this case was not evaluated, but the following check was carried out. As mentioned earlier, the numerical scheme in the interior has been found to be highly accurate. No artificial boundaries would be needed if it were economical to extend the limits of integration of the interior eq (4–6) far enough so that reflection from artificial boundaries could not reach the interior during the period of interest. In the check, the grid size was increased from (25×25) to (49×49), and the same disturbance as before was put in the (25×25) central region of the larger grid. The rest of it was filled with zeros, to effect the same flat external conditions simulated by condition (10) above. No reflection from the new boundaries could arrive at the interior (25×25) region before 30 time steps.

The comparison of the two computations through this time step is surprisingly close, even at the boundaries. The only discrepancy is that the water level in the middle of the smaller grid becomes slightly positive again past time step 7. In the larger grid check case, the water level

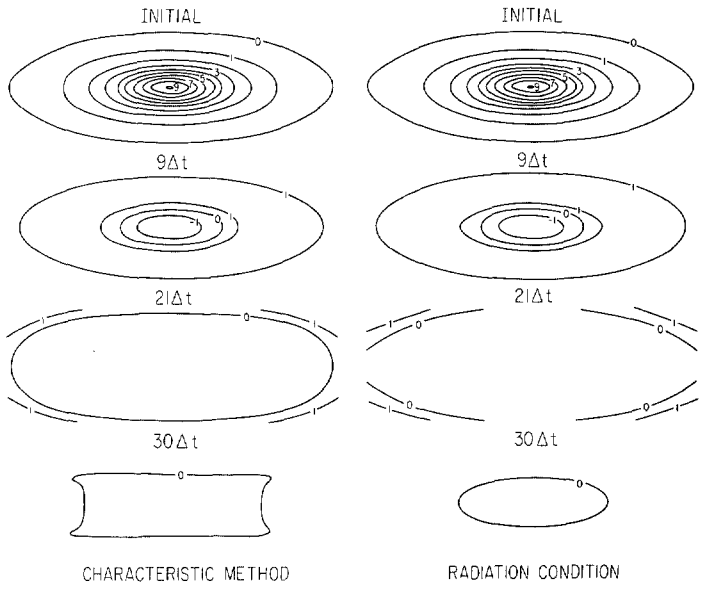

FIGURE 4.—Experiment 2 time evolution in two dimensions of the free surface elevation from the initial conditions $\eta=150/[15+(j-13)^2+(k-13)^2]-150/159$ for $\sqrt{(k-13)^2+(j-13)^2}<12$ and $\eta=0$ otherwise. The fields on the left were computed by the characteristic method as described. Those on the right, for comparison, were computed from the radiation condition method, an account of which is given in connection with experiment 3.

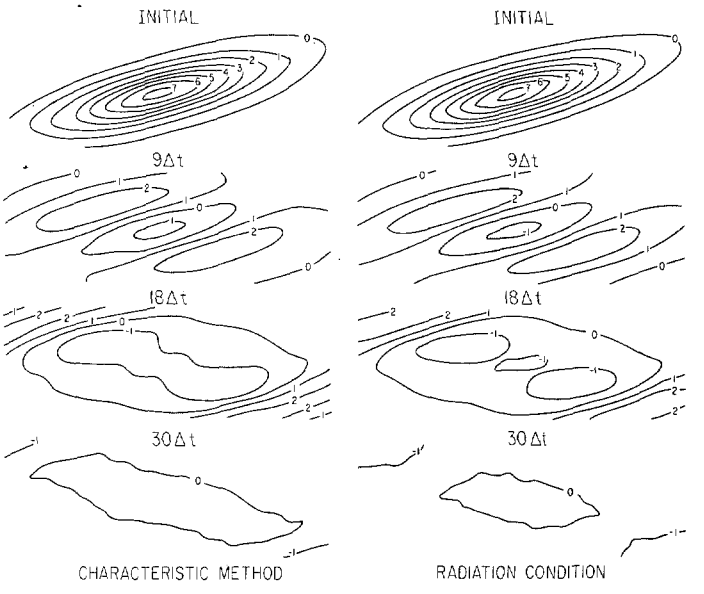

FIGURE 5.—Experiment 2, same as figure 4 with the initial disturbance elongated and skewed.

remains slightly negative at this time. This small difference is evidently due to boundary reflection; but in this case, it seemed negligible.

The fall of the water below equilibrium level is physically real, and it is an instance of the above-mentioned failure of Huygen's principle in two-space dimensions.

A similar but somewhat more exacting test is achieved by elongating the initial disturbance and skewing it with respect to the axes. The results were equally successful (fig. 5).

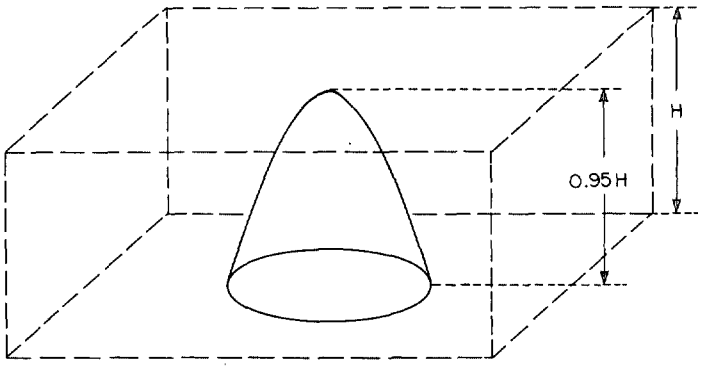

FIGURE 6.—Experiment 3, geometric configuration showing the four open boundaries and the sea mound of the form $h=H-0.95\times H\cos(\pi\sqrt{(k-13)^2+(j-13)^2}/10)$ for $\sqrt{(k-13)^2+(j-13)^2}<5$ and $h=H$ otherwise.

EXPERIMENT 3

A problem of oceanographic interest requiring open boundaries is that of a specified flow or wave form entering a region from outside as a function of time. This experiment was one in which a sea mound was placed in the middle of the grid to disturb such an impinging flow (fig. 6). The constant depth of the water outside a circle of radius 5 grid points from the center is 100 m. This means that approximately 85 percent of the area of integration was of constant depth. A plane wave was imposed at the left boundary, propagating into a region initially undisturbed. The method for handling the boundaries here is not quite as straightforward as in the previous case, and the left boundary is not really open to outgoing waves. An attempt to solve the problem using condition (10) on the *total* transport at the upper and lower boundaries proved to be numerically unstable. A linear stability analysis showed that this was because the forcing was parallel to the boundaries. The approach suggested by this analysis was to split the disturbance into two parts along these boundaries when applying (10). At the right and left boundaries, this refinement was not needed. The method finally used is outlined below.

At $j=0$ (left boundary):

$$U(0,y,t)=300\sin(\pi n/12).$$

Predict V from

$$\Delta_n V^n_{j,k}=\alpha\delta_k\eta^n_{j,k},\quad \alpha=-\frac{gh\Delta t}{2\Delta s}.$$

Obtain η from

$$\eta(0,y,t)=\pm\sqrt{U^2+V^2}/c.$$

At $k=0$, K (lower and upper boundaries): Predict U from

$$\Delta_n U^n_{j,0}=\alpha\delta_j\eta^n_{j,k}$$

and V from

$$\Delta_n V^n_{j,0}=\beta\Delta_k\eta^n_{j,k},\quad \beta=-\frac{gh\Delta t}{\Delta s}.$$

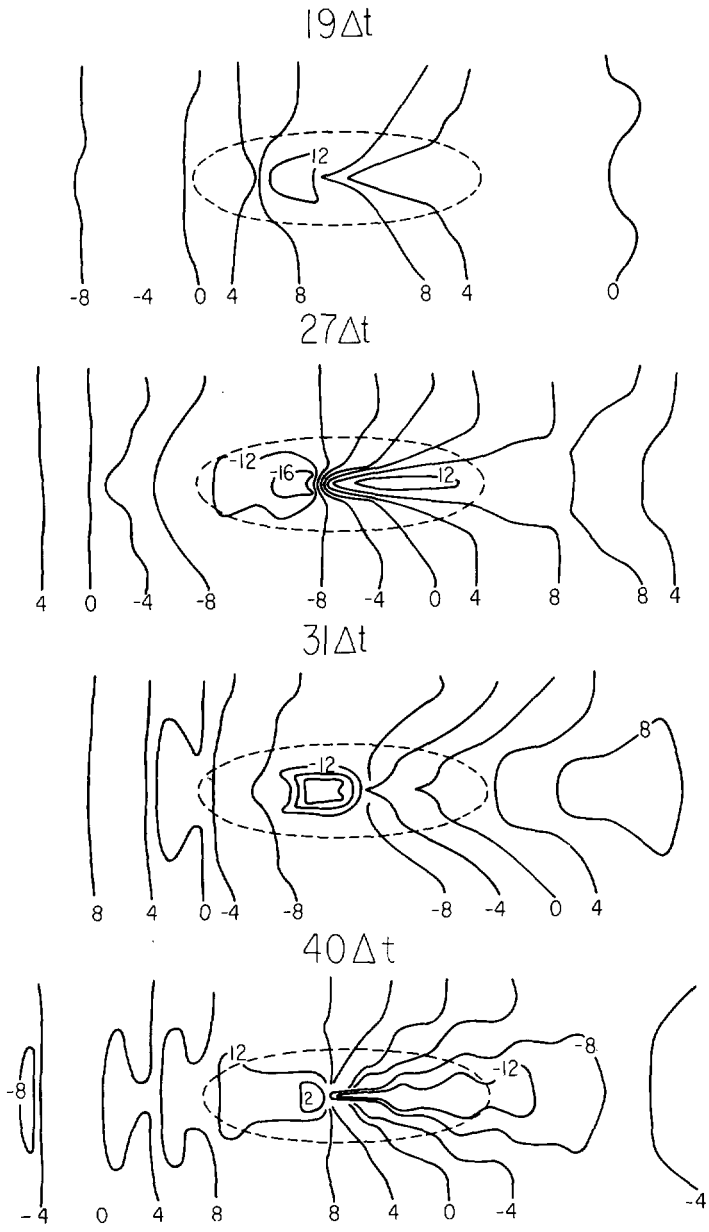

FIGURE 7.—Experiment 3, time evolution of the free surface elevation. The perimeter of the base of the mound is shown by the dashed line.

Then define

$$U'=U^n_{j,0}-U(0,y,-x/c+t),$$

and obtain η from

$$\eta=U(0,y,-x/c+t)/c\pm\sqrt{U'^2+V^2}/c,$$

and similarly for $k=K$.

At $j=J$ (right boundary):

Predict U from

$$\Delta_n U^n_{J,k}=\beta\Delta_j\eta^n_{J,k}$$

and V from

$$\Delta_n V^n_{J,k}=\alpha\delta_k\eta^n_{J,k}.$$

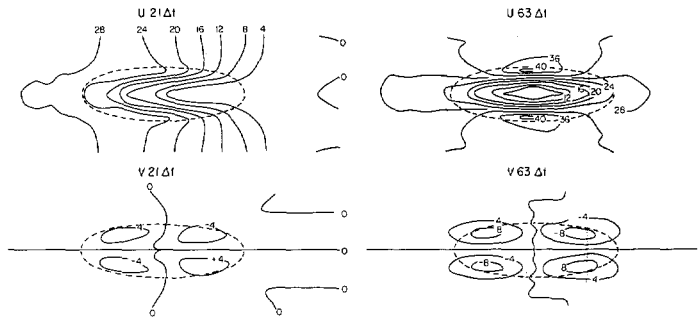

FIGURE 8.—Experiment 4, time evolution of the transports. The perimeter of the base of the mound is shown by the dashed line.

Obtain η from

$$\eta=\pm\sqrt{U^2+V^2}/c.$$

On each of the above boundary points where η is determined as a square root with a $\pm$ sign, the sign is determined by the direction of the transport. The plus sign was taken for outward transport and the minus sign for inward transport to maintain consistency with the assumption of no inflow other than that specified on the left boundary. In the interior, eq (4–6) were used.

The evolution of the free surface is shown in figure 7. The results appear quite meaningful. It is interesting that the steep slope of the bottom near the center of the grid apparently causes no computational instability or computational modes. As the crests and troughs of the plane wave approach the mound, they are apparently quite strongly retarded. The solution becomes periodic with the period of the incident wave.

EXPERIMENT 4

A similar problem of flow over a sea mound that tends to a steady state is given by the boundary inflow

$$\begin{aligned} U(0,y,t)&=30\sin(\pi n/36) && n\leq 18\\ &=30 && n\geq 18. \end{aligned}$$

All other parameters were as in experiment 3. Here, the approaching water is retarded up to about time step 30, after which the surface levels off and comes to a new equilibrium $\eta=30/\sqrt{100g}$.

Of special interest here are the transport fields (fig. 8). The U-component isolines wrap around the mound as might be expected, with a quasi-steady state being reached by 63 time steps. The V isolines also appear to be qualitatively reasonable, and by the time steady state is reached, they have maximum magnitude about one-fifth of the maximum U components.

This method of splitting up the waves is physically reasonable. It amounts to separating the wave perturbation into (1) the plane progressive wave components incident upon the region and (2) a reflected part. A similar technique was formalized by Vastano and Reid (1967) to study scattering of plane monochromatic waves by a circular island in water with sloping sides. In that work,

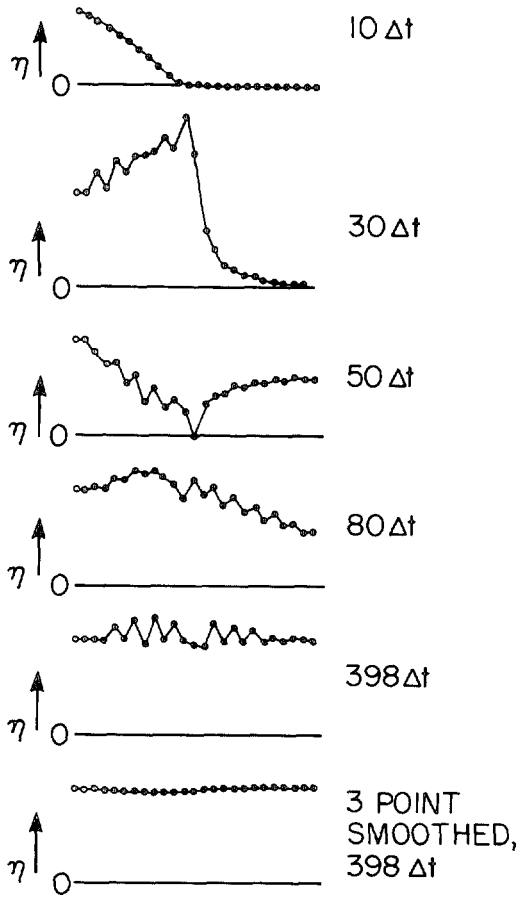

FIGURE 9.—Experiment 5, time evolution in one dimension of the free surface.

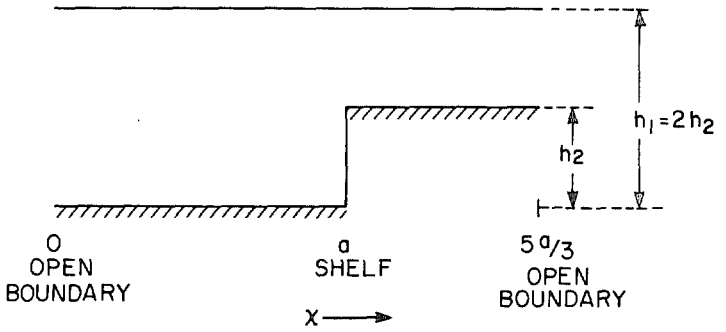

FIGURE 10.—Experiment 6, cross section showing the one-dimensional shelf and the open boundaries.

the reflected waves were handled by applying Sommerfeld's (1949) far-field radiation condition at the open boundaries. The sloping bottom and the island were axially symmetric and centered in a radial grid of otherwise constant-depth water. The constant-depth portion of the grid constituted 77 percent of the area of the integration, and the far-field radiation condition was applied at the perimeter of integration. Agreement with analytic solutions was good.

The radiation condition in two-space dimensions, as applied by Vastano and Reid, amounts to specifying an $r^{-1/2}$ asymptotic dependence for the scattered waves. Unlike the method of characteristics, it applies to a diverging flow; but it is an asymptotic condition and thus presumably requires a large grid. No systematic comparison has been made of these techniques; and, on balance, the choice in any particular computation probably will depend on the expected curvature of the wave fronts at the boundary relative to the grid resolution. Figures 4, 5, and 12 depict selected comparisons.

EXPERIMENT 5

Sommerfeld's condition cannot be used in one dimension, where reflected waves do not diminish as they travel from the source of reflection. To study the effectiveness of the characteristic method for one-dimensional physical reflection, the y variation of the sloping bottom was removed from experiment 3. Thus, the incident wave would not be dispersed in two dimensions; and the solution should not develop any y dependence. The mound thus became a ridge parallel to the y axis, with a crest reaching to within 5 percent of the water surface.

The results of this experiment for the same incident wave as that of experiment 4 are shown in figure 9. It can be seen that the water piles up to the left of the ridge but later reaches an equilibrium level. In addition, large-amplitude waves of length $2\Delta s$ begin to develop as the computation continues. It was not clear whether these computational modes resulted mainly from the sharpness of the sloping bottom or from the large ratio of the depth in the deepest part of the water to that in the shallowest portion.

This experiment demonstrates an important principle concerning the open boundary problem. The dispersion in a truly two-dimensional disturbance *reduces* the difficulty of treating boundaries effectively in the case of a specified inflow. In the physical situation, feedback from reflection is always present. To ignore it numerically at the inflow boundary is valid only to the extent that it is small; and in the one-dimensional case, there is no mechanism that reduces it asymptotically. Thus re-reflection at the inflow boundary in the one-dimensional case does appear to produce computational modes that were negligible in the two-dimensional computation.

EXPERIMENT 6

A one-dimensional problem with an analytic solution is provided by the discontinous bottom profile of figure 10. A monochromatic wave is specified to be incident upon the open boundary at $x=0$, and the shelf begins at $x=a$. Thus, the bottom slope was sharper than at any point in experiments 3–5, while the total change of depth was only about one-tenth as large.

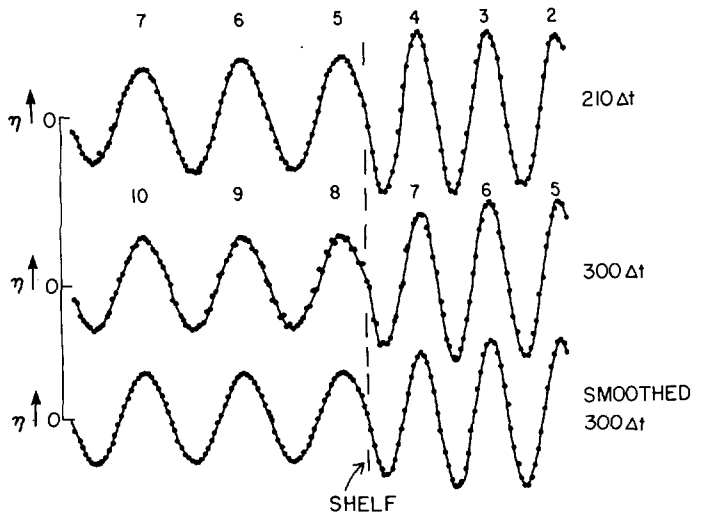

FIGURE 11.—Experiment 6, time evolution in one dimension of the free surface. The incoming wave crests are numbered as they enter the left boundary.

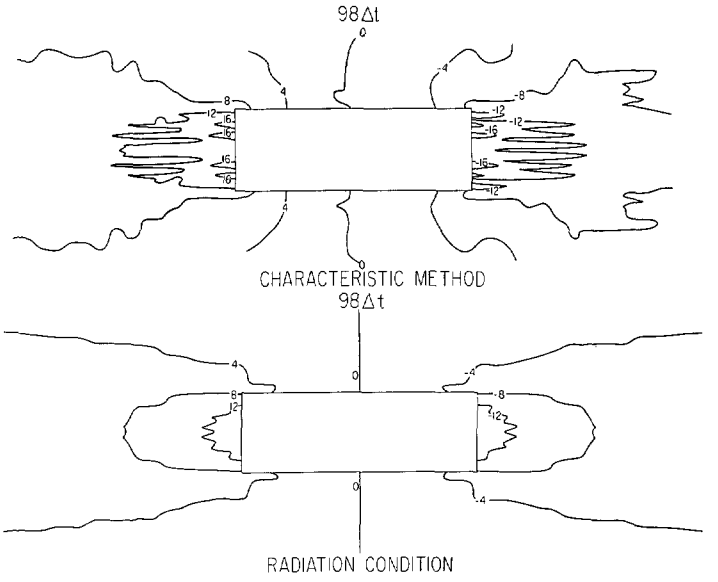

FIGURE 12.—Experiment 7, contours of free surface elevation at time step 98.

An analytic solution for this case can be expanded in the form

$$\eta \sim \sin \omega(t-x/c_1)-\lambda \sin \omega(t-x/c_1-2a/c_1)$$
$$+\lambda^2 \sin \omega(t-x/c_1-4a/c_1)- \ldots,$$
$$+\lambda \sin \omega(t+x/c_1-2a/c_1)-\lambda^2 \sin \omega(t+x/c_1-4a/c_1)+\ldots$$

where ω is the wave frequency and where only those terms are evaluated in which the arguments are positive, for the area to the left of the jump and

$$\eta \sim (1+\lambda)\{\sin \omega[t-(x-a)/c_2-a/c_1]$$
$$-\lambda \sin \omega[t-(x-a)/c_2-3a/c_1]$$
$$+\lambda^2 \sin \omega[t(x-a)/c_2-5a/c_1]- \ldots$$

for the region to the right of the jump where

$$\lambda=\frac{h_1c_2-h_2c_1}{h_1c_2+h_2c_1}=\frac{1-\sqrt{h_2/h_1}}{1+\sqrt{h_2/h_1}}.$$

These equations satisfy the conditions for given η at $x=0$ and the continuity of η and of U at $x=a$ up to terms of order λ^2. In the case of $h_2=\frac{1}{2}\ h_1$, λ is approximately $\frac{1}{6}$. This means that the reflection coefficient, which is approximately equal to λ, is also about $\frac{1}{6}$. The solution depends upon the relationship of a to the wavelength of the incident waves as well as upon the ratio of the depths. However, the amplitude is bounded so that, for a depth ratio of $\frac{1}{2}$, the amplitude on either side of the depth increment should not greatly exceed the amplitude of the incident waves. The amplitude over the shelf is always greater than the amplitude on the deeper water. Also, the waves should move more slowly in the shallower water, so the wavelength should be decreased there.

The results of this experiment are shown in figure 11. Here, 150 grid points were used in the direction of propagation, 90 located to the left of the depth increment and 60 to the right. The wavelength of the incident waves was 30 grid intervals. The solution shows that the waves come in smoothly at first, reaching the depth increment after about 90 time steps. The wave crests are numbered.

At 210 time steps, the solution was still quite smooth; and the second crest had almost reached the right open boundary. In the computations, this right boundary condition was specified by setting $U-c_2\eta=0$, the left by setting $U-c_1\eta=0$. Thus, the left boundary was effectively closed for the reflected outgoing waves. The effect of this is shown at time step 300 when the reflected waves have had time to return to that boundary. The computational mode of separated solutions at alternate grid points has reappeared, although not in as marked a fashion as in the previous experiment. However, it does not obscure the main features of the result; and a three-point smoothing produces a good result as shown.

EXPERIMENT 7

The scattering pattern of an island provides a more stringent test for our boundary conditions than that of a sea mound. In this experiment, the disturbance is caused by surface stress from a uniform wind field above the water. Identical experiments were run using both characteristic and radiation boundary conditions; the results are presented in figure 12.

As might be expected, the water piles up on the windward coast of the island. For a 40-km island and a depth of 100 m, for example, time step 98 corresponds to 1.1 hr. At this time, a 20 m/s wind has produced a rise in the water level of about 1.5 m. The sharp corners of the island seem to produce computational modes that the radiation boundary condition handles more effectively than the character-

istic boundary condition. At the time step shown, a signal would have traveled the distance from the open boundary to the island six times. Either computation could be easily improved by five-point smoothing.

4. CONCLUSIONS

The limitations of the methods discussed above should be emphasized. Both the characteristic method and the radiation condition method require the assumption of a region of constant depth near the boundary. (Edge waves are an important case thus excluded.) The former method is designed for situations in which the disturbance approaching the boundary can be considered locally at every boundary point as a plane wave. The latter applies when a radially symmetric wave is the better approximation. When the disturbance is composed of two plane-waves, the problem is tractable according to either method discussed in experiments 3 and 4 when one of the waves is known. When the noninteracting waves are both unknown, there is no available method for resolving them.

Vorticities introduced into the transport field by the stress field or by Coriolis effects are also beyond the scope of the methods. However, a considerable variety of problems, as indicated by the experiments, can be handled by either method, and important one-space-dimensional cases by the characteristic method. Practical applications of these open-boundary techniques in some operational storm-surge forecast programs may be possible.

ACKNOWLEDGMENTS

This work was supported at its inception by Contract Nonr-4756(00) and later by NSF G-10167. We gratefully acknowledge the generous cooperation of the Campus Computing Network of the University of California, Los Angeles.

In the technical development, we have profited by discussions with Prof. A. Arakawa and Dr. L. Greenstone.

REFERENCES

Garabedian, P. R., *Partial Differential Equations*, John Wiley & Sons, New York, N.Y., **1964**, 672 pp.

Platzman, George W., "The Computational Stability of Boundary Conditions in Numerical Integration of the Vorticity Equation," *Archiv für Meteorologie, Geophysik und Bioklimatologie*, Ser. A, Vol. 7, Vienna, Austria, **1954**, pp. 29–40.

Sielecki, Anita, "An Energy-Conserving Difference Scheme for the Storm Surge Equations," *Monthly Weather Review*, Vol. 96, No. 3, Mar. **1968**, pp. 150–156.

Sommerfeld, A., *Partial Differential Equations*, Academic Press, New York, N.Y., **1949**, 333 pp.

Trulio, John G., and Wallitt, Leonard, "Numerical Calculations of Viscous Compressible Flow Around a Stationary Cylinder," *NASA Contractor Report* No. 1465, Contract No. NAS8-18034, National Aeronautics and Space Administration, Washington, D.C., **1970**, 99 pp.

Vastano, A. C., and Reid, R. O., "Tsunami Response for Islands: Verification of a Numerical Procedure," *Journal of Marine Research*, Vol. 25, No. 2, New Haven, Conn., **1967**, pp. 129–139.

[*Received October 31, 1969; revised October 12, 1970*]